Optics Letters

Modal analysis of antiresonant hollow core fibers using S^2 imaging

Amy Van Newkirk,* J. E. Antonio-Lopez, James Anderson, Roberto Alvarez-Aguirre, Zeinab Sanjabi Eznaveh, Gisela Lopez-Galmiche, Rodrigo Amezcua-Correa, and Axel Schülzgen

CREOL, College of Optics and Photonics, University of Central Florida, Orlando, Florida 32816, USA
**Corresponding author: amy.vannewkirk@knights.ucf.edu*

Received 25 May 2016; revised 15 June 2016; accepted 16 June 2016; posted 17 June 2016 (Doc. ID 267003); published 12 July 2016

We analyze the higher-order core mode content in various designs of antiresonant hollow core fibers using spatially and spectrally resolved imaging. Hollow core fibers have great potential for a variety of applications, and understanding their mode content is crucial for many of these. Two different designs of hollow core fibers are considered, the first with eight nontouching rings and the second with eight touching rings forming a closed boundary core. The mode content of each fiber is measured as a function of length and bending diameter. Low amounts of higher-order modes were found in both hollow core fibers, and mode specific and bending-dependent losses have been determined. This study aids in understanding the core modes of hollow core fibers and possible methods of controlling them.

OCIS codes: (060.2270) Fiber characterization; (060.2280) Fiber design and fabrication.

http://dx.doi.org/10.1364/OL.41.003277

Hollow core fibers (HCFs) based on the antiresonant effect are quickly gaining attention for their excellent guiding properties, such as low loss and wide transmission windows. The first HCFs to guide by the antiresonant effect were Kagome fibers [1,2], which extended the transmission bandwidth and reduced the field overlap with the glass structure when compared to photonic bandgap fibers [3]. These fibers achieve low propagation losses due to strong suppression of coupling between the core modes and any available mode in the surrounding of the core. In order to increase the inhibited coupling between the core and cladding, a negative curvature, or hypocycloid, HCF fiber was developed in both simplified designs [4] and full lattice Kagome designs [5]. It was found that the core boundary shape has a strong influence on the guidance properties of all HCFs, and its accurate control is required in order to achieve low propagation losses [6–10]. In antiresonant hollow core fibers (ARHCFs), strong coupling to the cladding structure only occurs around specific resonance wavelengths, leading to significant propagation losses of the core modes at these wavelengths. As these resonances are dependent on the thickness of the core wall, open boundary ARHCFs were proposed in order to maintain constant core wall thickness and increase the transmission bandwidth over closed boundary designs [11]. Extensive research in the design of ARHCFs has been done in both simulation and experiment in an attempt to reduce the overall attenuation and bend-induced losses, control dispersion, and shift the resonance wavelengths in order to provide customized ranges of high transmission [12–18]. While many of these fibers' guidance characteristics have been studied in detail, the higher-order mode (HOM) content has not been looked at in depth experimentally. They are generally assumed to be approximately single mode, mostly determined from camera images of the near field [11,19] or recently, through selective excitation of the HOMs [20]. Understanding the mode content of ARHCFs is crucial for their applications, which include high-power delivery [21], UV and mid-IR transmission [11,19], sensing [22], nonlinear fiber optics [23], and in-fiber gas lasers [24].

Here we show an analysis on the mode content of two geometric designs of antiresonant hollow core fibers, which were both fabricated in-house. Using spatially and spectrally resolved imaging (S^2), the number of guided modes as well as the distribution of power between them can be accurately measured [25,26]. S^2 uses both the spatial and the spectral interference produced by the propagation of multiple modes in few-mode fibers to simultaneously image all of the supported modes and measure their relative intensities. This method has been used to measure passive and rare-earth-doped large-mode-area fibers, few-mode fibers for space-division multiplexing, photonic bandgap fibers, and more [27–30].

First, we examined a fiber with eight nontouching rings surrounding the air core. The core of the fiber is 70 μm in diameter (measured between the inner edges of two opposing rings), the rings have a 19 μm inner diameter with a 1.2 μm glass wall thickness, and the outer diameter is 150 μm. The spectrum of light transmitted through 4 m of this fiber is shown in Fig. 1(a), along with a scanning electron microscope (SEM) image of the fiber facet. Two resonances located at 850 and 1250 nm are clearly visible. These resonance wavelength locations can be predicted from the following equation:

$$\lambda_m = \frac{2t}{m}\sqrt{n^2 - 1}, \tag{1}$$

where t is the wall thickness of the rings, m is the order of the resonance (1, 2, 3…), and n is the index of refraction of the

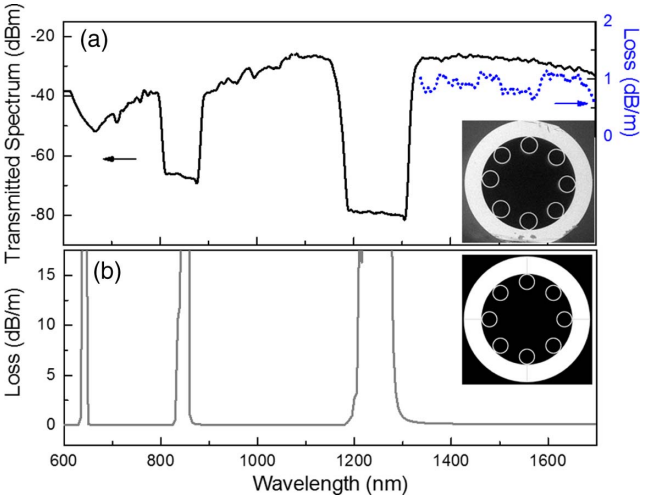

Fig. 1. (a) Transmitted white-light spectrum of 4 m of nontouching ring HCF (black) with a measured loss spectrum (blue dash) and an SEM facet image. (b) Simulated loss spectrum from COMSOL with the fiber design inset.

rings [31]. Using a cut-back measurement, a total propagation loss of 0.68 dB/m was measured around 1500 nm, and a partial loss spectrum is shown in Fig. 1(a). In order to verify the experimental results and gain predictive capabilities, simulations were performed using COMSOL Multiphysics. The nontouching ring fiber was created, shown in the inset of Fig. 1(b), and the loss spectrum of its fundamental mode was calculated. A maximum element size of 2λ in the air regions and $\lambda/5$ in the silica capillaries was used, with perfectly matched layer boundary conditions applied to the outer jacketing tube. The calculated loss spectrum is presented in Fig. 1(b), beneath the measured transmission spectrum of the fiber. Clearly, the resonances appear at the same locations, corresponding to the wall thickness of the rings.

The S^2 measurement setup is illustrated in Fig. 2. A supercontinuum source (NKT Photonics SuperK Compact) is used as the broadband light source, a single-mode fiber (SMF) is used as the excitation fiber, a microscope objective (MO) and lens (L) are used in a 4-f configuration to image the near field of the ARHCFs on a CCD as well as on the facet of the S^2 collection fiber (CF, a 50 μm graded index fiber), using a 50/50 beam splitter (BS). This enables a visual check on the input alignment conditions, e.g., the verification that most of the light is launched into the fundamental mode. The S^2 measurement is then performed as the collection fiber scans across the image of the ARHCFs facet on a 2D translation stage while the optical spectrum analyzer (OSA) measures the spectral interference at each location. All S^2 measurements shown for this fiber were measured for 1400–1600 nm, as this range is spectrally flat and far from the fiber's resonances.

The HOMs present after propagation through various lengths of the nontouching ring HCF and their dependence on bending were investigated using this method. Figure 3 shows the Fourier spectra after propagating through 3.35 m of this fiber straight and bent to a diameter of 55 cm. The straight fiber clearly shows three peaks in the Fourier spectrum. These peaks correspond to the group delay difference (GDD) between the fundamental mode and the respective HOM with intensity distributions shown above them. Asymmetry in the drawn fiber is the assumed reason for the difference in effective index of the two LP_{02}-like modes. The power in each of these three modes is less than 1%, with about 0.7% in LP_{11} and 0.3% in each of the LP_{02} modes, calculated with the method described by Nicholson *et al.* [25]. As the ARHCF is bent, the first two HOM peaks drop into the noise, and the third shifts in GDD. This shows that the bending caused the power in the first two HOMs to be coupled out of the core, while the effective refractive index difference between the fundamental mode and the second LP_{02} mode decreased.

A dependence of the HOM content on the fiber length of the nontouching ring fiber was then investigated by analyzing the S^2 measurements. Figure 4 shows the Fourier spectra of two of these measurements, taken as the length of the straight fiber was cut from 3.2 m down to 2 m. The same three HOM peaks are clearly visible, but a notable change in the peak height of the LP_{02} modes can be seen as the HCF was cut to 2 m. The height of the LP_{11} peak did not change significantly, indicating that the propagation loss of this mode is similar to the propagation loss of the fundamental mode. The above-mentioned total loss measured from a cut-back of this fiber was 0.68 dB/m in the region from 1400–1600 nm, and these data are shown as the black squares in the inset of Fig. 4. The loss of the combined LP_{02} modes was found to be approximately 4.2 dB/m from the S^2 measurement, corresponding to the red circles in the inset. When the length of this fiber was cut to 0.5 m, the power in the higher-order modes increased significantly, and several more modes appeared at higher GDDs. At this short length

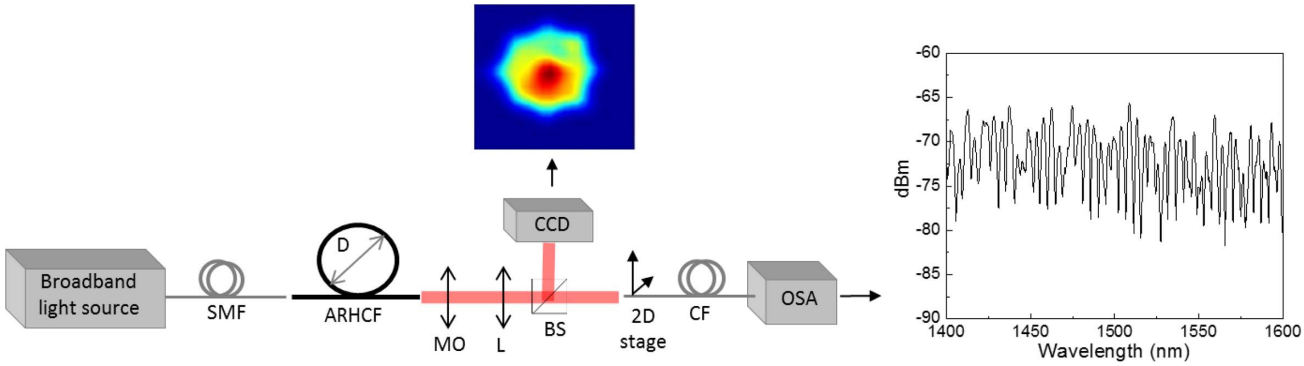

Fig. 2. Experimental setup used for S^2 measurement. An example near field of the nontouching ring ARHCF is shown above the CCD and an example transmitted light spectrum with multimode interference is shown next to the OSA.

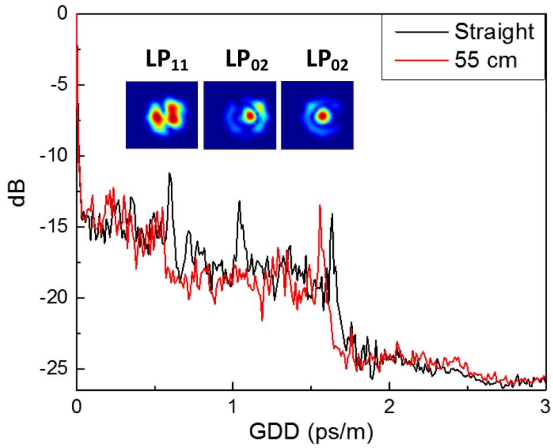

Fig. 3. Fourier spectra of straight and bent nontouching ring HCF, with mode images above the corresponding peaks.

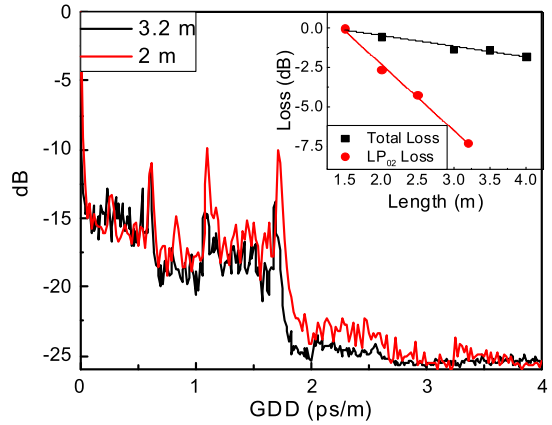

Fig. 4. Fourier spectra of two lengths of nontouching ring HCF. (Inset) Loss cut-back measurements.

of ARHCF, only approximately 50% of the light was guided in the fundamental mode, while the rest was divided among five HOMs.

In addition to calculating the fundamental mode loss as a function of wavelength, see Fig. 1(b), the loss of the first few HOMs was also calculated using COMSOL at the wavelength of 1550 nm. The loss of LP_{11} was found to be 0.6 dB/m, which is similar to the experimentally measured total loss of this fiber, 0.68 dB/m integrating from 1400 to 1600 nm. This agrees with the S^2 measurement, where no significant change in the amplitude of the LP_{11} peak was observed as the fiber was cut from 3.2 m to 1.5 m. The loss of the LP_{02} mode at 1550 nm was calculated to be 3.7 dB/m. Again, this is comparable to the measured loss obtained from the S^2 measurement, approximately 4.2 dB/m. Our simulation shows that the loss values calculated from S^2 agree with the theoretical predications. The only major difference was the loss of the fundamental mode, which simulation calculated to be just 0.13 dB/m at 1550 nm. The measured loss is higher than this theoretical value due to imperfections in the drawn fiber which increase the overall attenuation.

The measurements on this fiber show that HOMs are in fact supported and can propagate in the core of the ARHCF. While at a length of 3.35 m more than 98% of the power is in the fundamental mode, this low HOM content can still have a significant impact depending on the application of the ARHCF. This HOM content can be further mitigated by either bending the fiber, or by using longer lengths.

Next, an ARHCF with touching capillaries that form a closed core boundary was investigated. An SEM image of the fiber is shown in the inset of Fig. 5. The core is 48 μm in diameter (measured between the inner edges of two opposing capillaries), the capillaries are 30 μm along the long axis (radial direction), the thickness of the capillaries is 770 nm, and the outer diameter of the fiber is 150 μm. The light transmitted through 4 m of fiber is shown in Fig. 5. Due to the locations of the resonances of this fiber, it was investigated in the region from 1100–1300 nm by S^2 imaging. The total propagation loss measured in this wavelength range was 1.1 dB/m, and the loss spectrum in this region is included in Fig. 5. A 4 m long piece of the ARHCF was measured straight and bent at various bending diameters. Figure 6 shows the corresponding Fourier spectra of the straight fiber and bent to a diameter of 75 cm. Only one peak was visible, and the reconstructed LP_{11}-like mode image is shown above it. As the fiber is bent, the GDD of the LP_{11} mode shifts to smaller values, similarly to the nontouching ring ARHCF discussed above. In addition to shifting in the GDD, the intensity of the peak decreases with decreasing bending diameter, showing the increased coupling of the LP_{11} mode to cladding modes of the fiber as bending causes changes in the effective refractive indices of the core and cladding modes. The dependence of the power in LP_{11} is shown in the inset of Fig. 6 as a function of the inverse bending diameter. With 4 m straight, the relative power in the LP_{11} mode was very low, approximately 0.01%. As the fiber is bent to a diameter of 35 cm, this power decreases to 0.001%.

The length dependence of the HOM content was also determined with a cut-back S^2 measurement. As expected, Fig. 7 shows an increase in the peak intensity of the LP_{11} mode as the fiber is cut to a shorter length. Shown in the inset of Fig. 7 is a comparison of the total loss measured in a cut-back measurement (black squares), and the loss of power in LP_{11} obtained from the S^2 measurement (red circles). The estimated loss of the LP_{11} mode (red line in the inset) is 3.7 dB/m, which

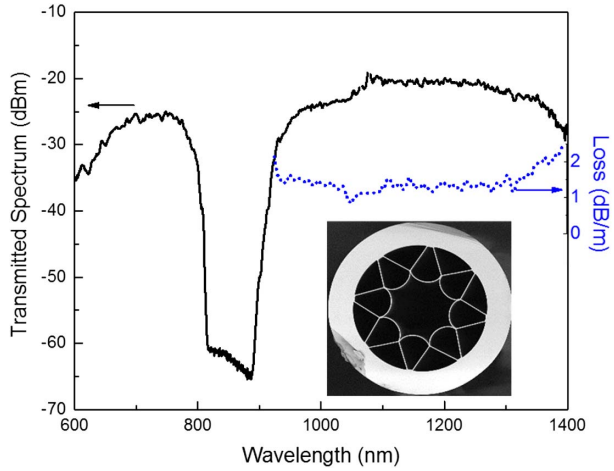

Fig. 5. Transmitted white-light spectrum of 4 m of the touching ring HCF (black) and loss spectrum (blue dash). (Inset) SEM image of the fiber facet.

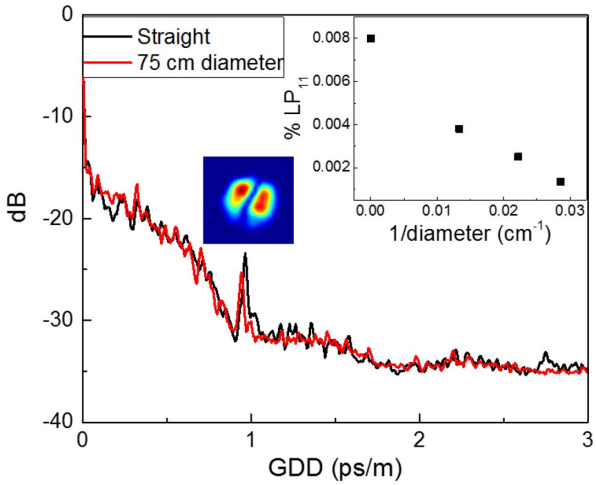

Fig. 6. Fourier spectra of straight and bent touching ring HCF, with mode images above the corresponding peaks. (Inset) LP_{11} power with inverse bending diameter.

is much higher than the total propagation loss of 1.1 dB/m. At a length of only 1 m, the power in LP_{11} was still relatively low, at a value of about 0.9%.

In conclusion, we have, to the best of our knowledge, experimentally measured the mode content of ARHCFs using spatially and spectrally resolved imaging for the first time. Both fibers analyzed showed some HOM content, with the majority of the light being guided in the fundamental mode. The HOM content found in the core of the closed boundary fiber was significantly lower than that measured in the nontouching ring fiber. This is most likely due to the ratio of the cladding element diameter to the core diameter, as it was found that a ratio of 0.68 was optimal for coupling the LP_{11} mode into the cladding mode, and the closed boundary fiber is much closer to that value [20]. Both fibers showed that, in general, the HOMs had higher bending loss and propagation loss than the fundamental mode, enabling possible mitigation of these modes through bending or using longer lengths of ARHCF. While the fundamental mode losses of the fibers shown here (~1 dB/m) and the HOM losses (~4 dB/m) allow for sufficiently single-mode

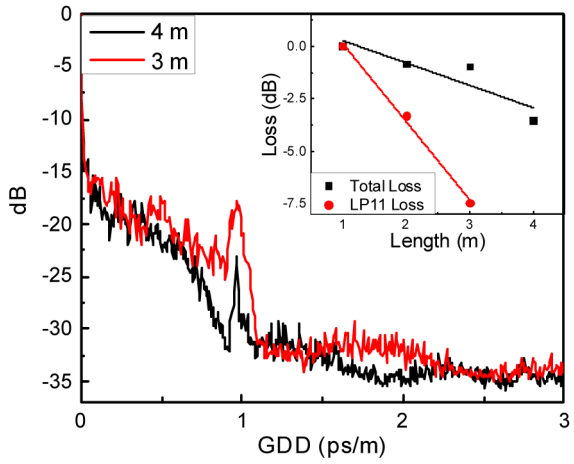

Fig. 7. Fourier spectra of two lengths of touching ring HCF. (Inset) Loss cut-back measurements.

operation after a few meters of ARHCF, much lower fundamental mode losses and higher HOM extinction ratios have been shown to be possible. Recently, we have fabricated an ARHCF with a propagation loss of 70 dB/km and a HOM loss ratio of over 150. Also, simulations have shown HOM extinction ratios over 500 for a nested antiresonant nodeless HCF [17] and 1200 for a six-ring open boundary ARHCF [20].

Funding. Army Research Office (ARO) (W911NF-12-1-0450, W911NF-15-1-0338); Air Force Office of Scientific Research (AFOSR) (FA9550-15-10041).

REFERENCES

1. F. Benabid, J. C. Knight, G. Antonopoulos, and P. St.J. Russell, Science **298**, 399 (2002).
2. F. Couny, F. Benabid, and P. S. Light, Opt. Lett. **31**, 3574 (2006).
3. C. M. Smith, N. Venkataraman, M. T. Gallagher, D. Müller, J. A. West, N. F. Borrelli, D. C. Allan, and K. W. Koch, Nature **424**, 657 (2003).
4. A. D. Pryamikov, A. S. Biriukov, A. F. Kosolapov, V. G. Plotnichenko, S. L. Semjonov, and E. M. Dianov, Opt. Express **19**, 1441 (2011).
5. Y. Y. Wang, N. V. Wheeler, F. Couny, P. J. Roberts, and F. Benabid, Opt. Lett. **36**, 669 (2011).
6. R. Amezcua-Correa, N. G. R. Broderick, M. N. Petrovich, F. Poletti, and D. J. Richardson, Opt. Express **14**, 7974 (2006).
7. M. S. Habib, O. Bang, and M. Bache, Opt. Express **24**, 8429 (2016).
8. F. Poletti, N. V. Wheeler, M. N. Petrovich, N. Baddela, E. Numkam Fokoua, J. R. Hayes, D. R. Gray, Z. Li, R. Slavík, and D. J. Richardson, Nat. Photonics **7**, 279 (2013).
9. P. J. Roberts, F. Couny, H. Sabert, B. J. Mangan, D. P. Williams, L. Farr, M. W. Mason, A. Tomlinson, T. A. Birks, J. C. Knight, and P. St.J. Russell, Opt. Express **13**, 236 (2005).
10. W. Belardi and J. C. Knight, Opt. Express **21**, 21912 (2013).
11. A. N. Kolyadin, A. F. Kosolapov, A. D. Pryamikov, A. S. Biriukov, V. G. Plotnichenko, and E. M. Dianov, Opt. Express **21**, 9514 (2013).
12. W. Belardi, J. Lightwave Technol. **33**, 4497 (2015).
13. W. Belardi and J. C. Knight, Opt. Lett. **39**, 1853 (2014).
14. W. Belardi and J. C. Knight, Opt. Express **22**, 10091 (2014).
15. A. Hartung, J. Kobelke, A. Schwuchow, J. Bierlich, J. Popp, M. A. Schmidt, and T. Frosch, Opt. Lett. **40**, 3432 (2015).
16. F. Yu and J. C. Knight, Opt. Express **21**, 21466 (2013).
17. F. Poletti, Opt. Express **22**, 23807 (2014).
18. F. Yu and J. Knight, IEEE J. Sel. Top. Quantum Electron. **22**, 1 (2015).
19. A. Hartung, J. Kobelke, A. Schwuchow, K. Wondraczek, J. Bierlich, J. Popp, T. Frosch, and M. A. Schmidt, Opt. Express **22**, 19131 (2014).
20. P. Uebel, M. C. Günendi, M. H. Frosz, G. Ahmed, N. N. Edavalath, J.-M. Ménard, and P. St.J. Russell, Opt. Lett. **41**, 1961 (2016).
21. M. Michieletto, J. K. Lyngsø, C. Jakobsen, J. Lægsgaard, O. Bang, and T. T. Alkeskjold, Opt. Express **24**, 7103 (2016).
22. G. Tsiminis, K. J. Rowland, E. P. Schartner, N. A. Spooner, T. M. Monro, and H. Ebendorff-Heidepriem, Opt. Express **24**, 5911 (2016).
23. P. St.J. Russell, P. Hölzer, W. Chang, A. Abdolvand, and J. C. Travers, Nat. Photonics **8**, 278 (2014).
24. M. R. Abu Hassan, F. Yu, W. J. Wadsworth, and J. C. Knight, Optica **3**, 218 (2016).
25. J. W. Nicholson, A. D. Yablon, S. Ramachandran, and S. Ghalmi, Opt. Express **16**, 7233 (2008).
26. C. Jollivet, D. Flamm, M. Duparré, and A. Schülzgen, J. Lightwave Technol. **32**, 1068 (2014).
27. J. W. Nicholson, A. D. Yablon, J. M. Fini, and M. D. Mermelstein, IEEE J. Sel. Top. Quantum Electron. **15**, 61 (2009).
28. J. Bromage, J. M. Fini, C. Dorrer, and J. D. Zuegel, Appl. Opt. **50**, 2001 (2011).
29. F. Kong, K. Saitoh, D. Mcclane, T. Hawkins, P. Foy, G. Gu, and L. Dong, Opt. Express **20**, 26363 (2012).
30. C. Jollivet, B. Samson, L. Leick, L. Shah, M. Richardson, and A. Schülzgen, Opt. Eng. **54**, 011006 (2014).
31. J.-L. Archambault, R. J. Black, S. Lacroix, and J. Bures, J. Lightwave Technol. **11**, 416 (1993).